Interfacial thermal resistance between carbon nanotubes: Molecular dynamics simulations and analytical thermal modeling

Hongliang Zhong and Jennifer R. Lukes*
Department of Mechanical Engineering and Applied Mechanics, University of Pennsylvania, Philadelphia, Pennsylvania 19104, USA
(Received 27 December 2005; revised manuscript received 29 May 2006; published 1 September 2006)

Interfacial thermal transport between offset parallel (10,10) single-wall carbon nanotubes is investigated by molecular dynamics simulation and analytical thermal modeling as a function of nanotube spacing, overlap, and length. A four order of magnitude reduction in interfacial thermal resistance is found as the nanotubes are brought into intimate contact. A reduction is also found for longer nanotubes and for nanotubes with increased overlap area. Thermal resistance between a nanotube and a reservoir at its boundary increases with decreasing reservoir temperature. Additionally, length-dependent Young's moduli and damping coefficients are calculated based on observed nanotube deflections.

DOI: 10.1103/PhysRevB.74.125403 PACS number(s): 66.70.+f, 05.10.−a, 62.25.+g, 68.35.Md

I. INTRODUCTION

Due to their superior thermal conductivity,[1–7] single-wall carbon nanotubes (SWNTs) have elicited great interest as potential thermal management materials, for example, as fillers in polymer composites[8] and as thermal interface materials.[9] Recent measurements on carbon nanotube suspensions and composites indicate that their effective thermal conductivities are lower than expected based on the high nanotube thermal conductivity[10] and that thermal resistance between the nanotube and the surrounding medium may be a key factor limiting heat flow.[11,12]

Another important but little-studied factor impacting the effective thermal conductivity of carbon nanotube-polymer composite materials is interfacial thermal resistance between carbon nanotubes. These composites are well known to exhibit percolation behavior (e.g., see Ref. 13), and correspondingly display an interconnected network structure in which individual nanotubes are in contact with other nanotubes as well as with the surrounding host material.[13,14] Nanotube-nanotube thermal resistances will also be important in buckypaper-based[15] materials. Additionally, phonons in suspended carbon nanotubes play an important role in mediating electron tunneling transport,[16] and it is expected that thermal/vibrational coupling between neighboring nanotubes in nanotube arrays will have a significant effect on the performance of devices based on these structures.

Few studies to date have discussed the interfacial resistance at the contacts between carbon nanotubes. Molecular dynamics simulations reveal that heat transport in aligned nanotube bundles is dominated by tube-tube interfacial resistance.[11] This may explain why the thermal conductivity of nanotube bundles is much lower than that of a single carbon nanotube.[17] No studies have yet been reported that investigate the dependence of nanotube-nanotube interfacial resistance on nanotube length or on overlap and spacing at the tube-tube junctions. These parameters can be varied experimentally; in particular, nanotube length can be controlled by chemical vapor deposition processing conditions,[18] and nanotube spacing and size can be controlled by the placement of catalyst.[19]

It is critically important to understand how length, spacing, and overlap influence energy transport so that enhancements in nanotube composite thermal conductivity beyond current levels can be achieved and so that a fundamental understanding of thermal and vibrational coupling between isolated, arbitrarily spaced carbon nanotubes can be attained. In addition, carbon nanotubes are of great interest as oscillators in mass detection and radio frequency signal processing.[20] Their mechanical properties will strongly impact quality factor and performance in these applications. Although such properties have been investigated by a number of groups for individual nanotubes (see Ref. 21 for a review), few systematic studies of size effects on mechanical properties have been performed. Such effects, particularly those related to aspect ratio, will become important design parameters as advances in synthesis and processing enable ever-improving control of nanotube structure and dimensions. Existing studies in this area have so far been limited to examination of the influence of diameter and wall thickness.[22–25] Little is known about the *length* dependence of carbon nanotube mechanical properties.

In this paper classical thermal modeling results that show the effect of nanotube length, overlap, and spacing on thermal interfacial resistance between two carbon nanotubes are presented. Also presented are the resistances at the boundary between a nanotube and a thermal reservoir for different temperatures and nanotube lengths. Finally, length-dependent mechanical properties estimated from the simulations are reported.

II. ATOMISTIC MODELING METHOD

Nonequilibrium molecular dynamics[26] is used to calculate temperature profiles in a system of offset parallel carbon nanotubes whose general configuration in terms of overlap and spacing is shown in the upper portion of Fig. 1. Spacing is defined as the smallest distance between the outer walls of opposing nanotubes and is measured from the centers of the atoms in those walls. The temperature profiles are then used to determine the interfacial thermal resistance between carbon nanotubes, as described in Secs. III and IV, for a variety of geometrical configurations. The initial configuration of a (10,10) SWNT is constructed using a bond length of 1.42 Å.

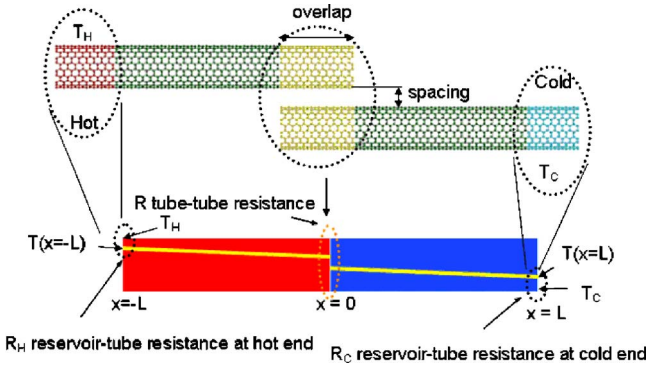

FIG. 1. (Color online) Correspondence between molecular dynamics (upper figure) and finite difference (lower figure) models. Two nanotubes are configured with a given overlap and spacing, which are varied to see the effect on tube-tube and reservoir-tube resistances. Hot and cold ends of the nanotubes are maintained at temperatures T_H and T_C, respectively.

The modeling procedure involves integration of Newton's classical equations of motion for atoms interacting with each other through an empirical interatomic potential. It does not explicitly model electrons and therefore cannot simulate electron-electron or electron-phonon interactions. Measurements indicate that the phonon contribution to thermal conductivity is dominant in both multiwall carbon nanotubes (MWNTs) and SWNTs at all temperatures,[27] which justifies neglecting electronic effects in simulations of carbon nanotubes. The carbon-carbon bonded interaction is modeled by the reactive bond order (REBO) potential.[28]

There is some variability in the literature regarding the representation of the nonbonded van der Waals interaction between individual carbon atoms in carbon nanotubes. Most commonly it has been expressed as a Lennard-Jones (LJ) potential,[29] but Morse potentials have also been used.[30] Qian *et al.*[31] have compared and discussed both of these representations at length. Among studies adopting the LJ potential

$$\phi(r) = 4\varepsilon\left[\left(\frac{\sigma}{r}\right)^{12} - \left(\frac{\sigma}{r}\right)^{6}\right] \tag{1}$$

to model carbon-carbon nonbonded interactions, at least nine distinct parameterizations have been utilized.[32–38] Here "distinct" is defined as either the energy parameter ε or the distance parameter σ varying more than 10% from any other parameterization. A parameterization frequently employed for LJ interactions is $\varepsilon=2.4$ meV and $\sigma=0.34$ nm; this is based on the compressibility and graphene layer spacing obtained from such parameters. The present study employs the parameterization used by Lu *et al.*,[33] $\varepsilon=4.41$ meV and $\sigma=0.228$ nm. An analysis exploring the effect of different parameterizations on thermal resistance is presented in Sec. VI.

Before the primary calculations begin, a simulation is run for each desired nanotube length with free boundary conditions. This is done to obtain the stress-free nanotube length, which differs negligibly from the original starting length. The simulations proper begin by equilibrating the system at 300 K with a Nosé-Hoover[39] thermostat for 400 ps. Then a small region at the left end of the left nanotube is raised to

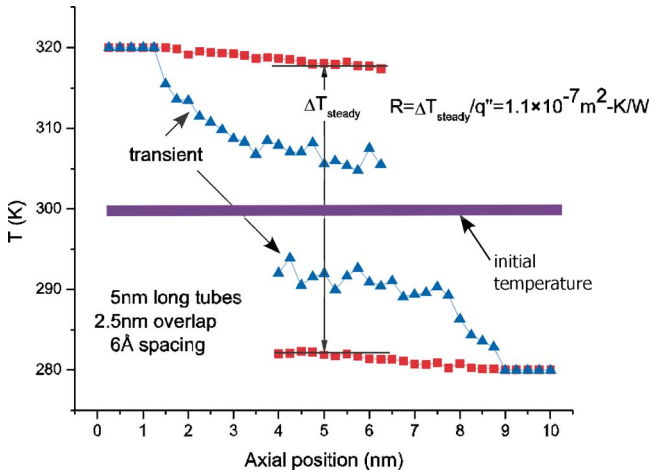

FIG. 2. (Color online) Initial (solid line), transient (triangles), and steady-state (squares) temperature profiles for two 5 nm long tubes with 2.5 nm overlap and 6 Å spacing. The outermost five data points at the left and right ends represent the temperatures imposed at the hot and cold reservoirs after initial thermalization of the system at 300 K. The steady-state temperature jump in the overlap region corresponds to tube-tube thermal resistance.

320 K and the corresponding region at the right end of the right nanotube is lowered to 280 K; the temperatures in these "reservoirs" are maintained throughout the simulation by Nosé-Hoover thermostatting. Variation of the thermostat parameters was not observed to cause any discernible change in the tube-tube or reservoir-tube resistances discussed in Secs. V and VII.

Outside the hot and cold regions, five rings of atoms at the outermost (nonoverlapping) end of each nanotube are fixed to prevent rotation and axial translation of the nanotubes. The transient local temperature is calculated for each ring of atoms using equipartition,

$$T = \frac{1}{3nk_B}\sum_{i=1}^{n} m_i v_i^2 \tag{2}$$

where each ring has n atoms with masses m_i and velocities v_i; and k_B is Boltzmann's constant. After hot and cold temperatures are imposed at the boundaries, the resultant thermal disturbances propagate inward from the boundaries toward the overlap region and the temperature profiles change over time from flat (300 K everywhere) to linear. Figure 2 illustrates the initial, transient, and steady-state temperature profiles for a system of two 5 nm long tubes with 2.5 nm overlap and 6 Å spacing.

III. THERMAL INTERFACIAL RESISTANCE

The representation of heat transfer across interfaces by a single parameter, the thermal interfacial resistance R, is well established in the literature.[40–43] This quantity is defined as

$$R = A\Delta T/q, \tag{3}$$

where ΔT is the steady-state temperature jump between the two surfaces forming the interface, A is the area of the inter-

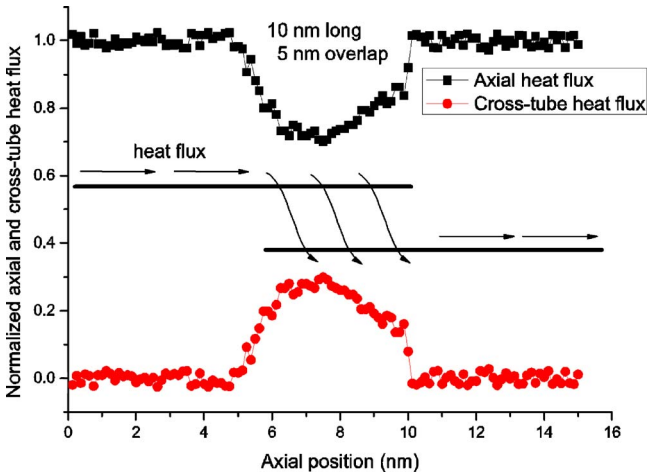

FIG. 3. (Color online) Local axial and cross-tube heat flux of each ring of atoms along the axial direction. The total length is 15 nm for two parallel 10 nm nanotubes that are placed with 5 nm overlap. The central dip indicates a decrease in axial heat flux corresponding to an increase in cross-tube heat flux.

face, and q is the heat flow rate across the interface.

Equation (3) is usually applied to systems with planar interfaces for which A is well defined and the heat flow is one-dimensional perpendicular to the interface. Previous studies of carbon nanotube thermal interfacial resistance have also employed the thermal boundary resistance concept.[11,12] In these studies, the nanotube was completely encapsulated either by other nanotubes[11] or by a fluid medium;[12] the interfacial area was reasonably chosen as the nanotube surface area for those systems. In the present problem of partially overlapping nanotubes, calculation of thermal interfacial resistance is complicated by two factors: (i) the overlap contact area A between two isolated cylindrical objects is not well defined geometrically, and (ii) the heat flow in the overlap region is multidimensional—it has axial and cross-tube components (Fig. 3).

We address this problem by representing the two-dimensional overlap region as a single planar interface between coaxial hot and cold nanotubes joined end to end (lower portion of Fig. 1). In this way, we map the multidimensional lateral interfacial heat flow problem onto a one-dimensional axial heat flow problem. Our one-dimensional model system is consistent with the one-dimensional systems for which thermal interfacial resistance is usually calculated, and the appropriate interfacial area to use in Eq. (3) for this system is perpendicular to the nanotube axis. The exact definition of this area is open to debate and has in previous molecular dynamics studies of thermal transport in (10,10) SWNTs been interpreted as the cross-sectional area occupied by nanotubes in bundles,[2] a flat ring of 1 Å thickness and circumference defined by the centers of the atoms around the nanotube,[4] a flat ring of thickness 3.4 Å and circumference defined by the centers of the atoms around the nanotube,[7] and, most commonly, a circle with circumference defined by the centers of the atoms around the nanotube.[3,5,6,44] The latter two definitions yield almost identical areas, $A=14.4\times10^{-19}$ m^2, so we have used this area in the present work. Thermal interfacial resistance is known to depend on the geometry of the contacting surfaces through surface roughness.[42] Similarly, the present calculations yield resistances that depend on the geometrical configuration of the interface, namely, nanotube overlap and nanotube spacing.

IV. ONE-DIMENSIONAL THERMAL RESISTANCE CALCULATION METHOD

Thermal interfacial resistances are calculated by fitting transient temperature profiles obtained by molecular dynamics to a finite difference solution of the one-dimensional heat equation. This method does not require that steady state be achieved in the molecular dynamics (MD) simulations, which, due to the L^2 dependence of thermal diffusion time, leads to significant computational savings. An alternative approach based on lumped thermal capacitance has been used previously to address this issue[10] but was not adopted due to the radial asymmetry of the present problem.

The carbon nanotubes are both governed by the one-dimensional transient heat conduction equation

$$k\frac{\partial^2 T}{\partial x^2}=\rho C_p\frac{\partial T}{\partial t}, \tag{4}$$

where the density $\rho=2243$ kg/m^3 is defined as nanotube mass divided by $L\cdot A$, and the specific heat C_p is 700 J/kg K.[45] Carbon nanotube thermal conductivity k has been found to be size-dependent,[6,7,46–48] so the k values used in solving Eq. (4) are drawn separately for each length from previous simulation data.[46,48] As in the molecular dynamics simulations, the end temperatures of both tubes in the finite difference model are fixed to $T_H=320$ K at the hot end and $T_C=280$ K at the cold end. It is important to note that although the parameters ρ, k, and R depend on the choice of A, area effects cancel in Eq. (4) and its boundary conditions [Eqs. (5)–(7) below] because the same reference area is used in each parameter.

As discussed above, the MD overlap region is collapsed to a single point $x=0$ to map it onto the one-dimensional heat equation (Fig. 1). The appropriate temperature jump/thermal resistance boundary condition at a one-dimensional (1D) interface is given as[49]

$$-k\left.\frac{\partial T}{\partial x}\right|_{0^-}=\frac{T(0^-)-T(0^+)}{R}=-k\left.\frac{\partial T}{\partial x}\right|_{0^+}. \tag{5}$$

Here we take 0^- and 0^+ as the end points at the contact between the hot and cold tubes, respectively (lower portion of Fig. 1). To verify the applicability of such a simple 1D model, the thermal extent of the overlap region was found from the molecular dynamics simulations by analyzing the local heat fluxes in each atomic ring of the nanotube. Significant cross-tube local fluxes were found inside the overlap region as shown in Fig. 3, but outside the overlap region heat flowed solely along the tube and the one-dimensional nature was preserved.

Thermal resistances between the thermostatted reservoirs and the nonthermostatted regions of the tube are also included in terms of the reservoir-tube temperature jumps,

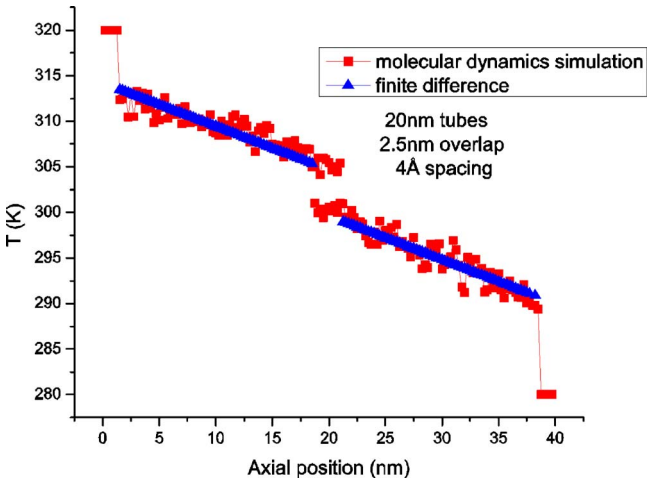

FIG. 4. (Color online) Transient temperature profile fit of finite difference model to molecular dynamics simulation data.

$$-k\left.\frac{\partial T}{\partial x}\right|_{-L} = \frac{T_H - T(-L)}{R_H}, \tag{6}$$

$$\frac{T(+L) - T_C}{R_C} = -k\left.\frac{\partial T}{\partial x}\right|_{+L}, \tag{7}$$

where $-L$ is the position of the hot nanotube–hot reservoir boundary, and $+L$ is that of the cold nanotube–cold reservoir boundary. L is not the tube length but the length from the edge of the nonthermostatted atoms to the starting position of the overlap region. R_H and R_C are the reservoir-tube resistances for the hot and cold ends, respectively. Boundary temperature jumps have been observed in conduction heat transfer in thin films[50] and are expected when ballistic phonon transport effects are nonnegligible. This condition is true in the present simulation, since the estimated phonon mean free path[27] is much longer than the nanotube length.

The tube-tube and reservoir-tube thermal interfacial resistances were determined by performing a least-squares fitting of the finite difference solution to the transient heat equation at a particular snapshot in time to the molecular dynamics simulations at the corresponding snapshot, as shown in Fig. 4. Here "snapshot" is defined as a 100 ps time window over which temperatures in each ring of the carbon nanotube are time averaged. Such averaging is necessary to reduce statistical noise and to enable a meaningful assignment of local temperature for fitting purposes. As the resistances are not initially known, initial guesses must be supplied to the fitting routine.

V. TUBE-TUBE INTERFACIAL RESISTANCES

This best fit procedure is done for several configurations of two carbon nanotubes of different tube lengths, overlaps, and spacings. Figure 5 shows the obtained tube-tube thermal resistances for nanotubes with 2.5 nm overlap. The resistances are the same order of magnitude as those obtained in related studies in the literature at comparable spacing (2–4 Å). Maruyama's MD simulations of (5,5) SWNTs in

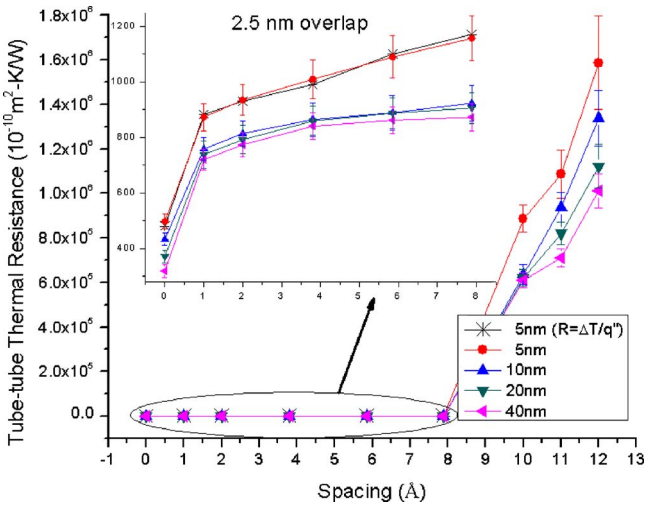

FIG. 5. (Color online) Tube-tube thermal resistance vs spacing and length for 5, 10, 20, and 40 nm nanotubes with 2.5 nm overlap. Asterisks are from steady-state MD simulations for 5 nm tubes; filled symbols are from finite difference fit to transient MD simulations. A four order of magnitude decrease in R is found as nanotube spacing decreases.

bundles[11] display a slightly lower SWNT-SWNT resistance value (6.46×10^{-8} m^2 K/W) than those found in the present work. Huxtable *et al.*[12] report interfacial resistances obtained both from MD simulations of the (5,5) SWNT-octane interface (4×10^{-8} m^2 K/W) and from short time scale optical absorption experiments probing the SWNT–sodium dodecyl sulfate interface (8.3×10^{-8} m^2 K/W), where coupling can occur only via low-frequency modes. As with Maruyama's study, their MD values are somewhat lower than the present ones, but their experimental measurements are in the same range.

The tube-tube thermal resistances for 5 nm long nanotubes both from steady-state molecular dynamics simulations and from the finite difference fit to transient molecular dynamics simulations are the same within error. The values obtained at different snapshots in time ranging from "450 ps" (400–500 ps time averaging) to "850 ps" (800–900 ps time averaging) were also the same within the calculation uncertainty [Fig. 6(a)]. These two observations justify our fitting method of calculating resistances.

Tube-tube resistance is observed to increase with spacing. This occurs because the van der Waals interactions, which provide the only heat transfer mechanism between the nanotubes, weaken with increasing distance. This increase of tube-tube thermal resistance is dramatic at large tube spacing, increasing four orders of magnitude as spacing increases from zero to 12 Å. The simulations were performed at a cutoff radius of 10 Å, beyond which the Lennard-Jones interaction is vanishingly small. Simulations at increasing cutoff radius from 12 Å to 20 Å were performed to determine the influence of this parameter on the simulation results, and negligible changes in the thermal interfacial resistances were found. Interestingly, the resistance continues to increase beyond 10 Å instead of jumping to infinity above this spacing. A possible explanation for finite resistance above the cutoff

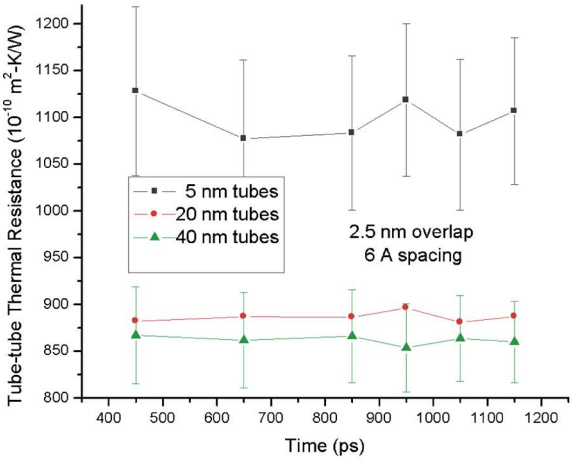

(a)

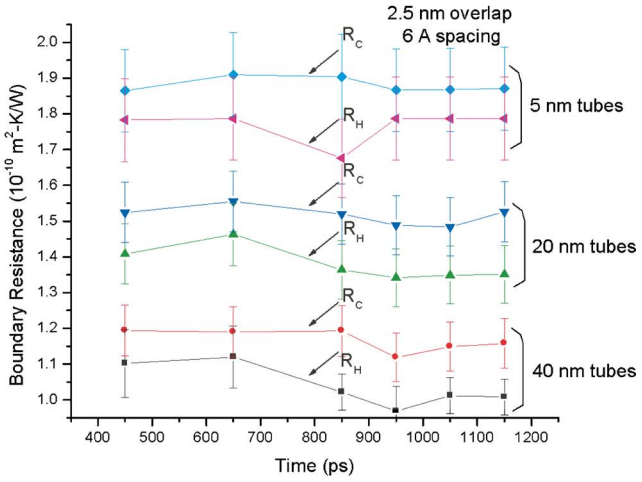

(b)

FIG. 6. (Color online) (a) Tube-tube and (b) tube-reservoir resistance vs fitting time. Each data point represents a snapshot in time at which the fitting is performed. No fitting time dependence is observed within the error of the calculations.

distance is that thermal fluctuations periodically bring atoms within the cutoff distance, enabling sporadic energy transfer from nanotube to nanotube. The thermal resistance decreases greatly when two carbon nanotubes are fused together. Those data points are represented as "0 Å" spacing in Fig. 5. Fused tubes are joined by a single row of carbon atoms in the overlap region. In fused tubes the heat transfer mechanism by bonded interactions is enabled, giving more efficient heat transfer and therefore smaller thermal resistance than nonfused nanotubes whose interactions are van der Waals only.

Tube-tube resistance decreases with tube length, an effect also seen in Fig. 7, which shows results for nanotubes spaced at 6 Å. A similar decrease for longer nanotubes was found by Huxtable *et al.*[12] for the SWNT-D_2O thermal resistance. The presence of more low-frequency phonon modes in the longer nanotubes[46,48] may enable increased tube-tube coupling, leading to reduced resistance. As overlap increases, the tube-tube resistance decreases because more atoms from opposing nanotubes are able to exchange heat through van der Waals

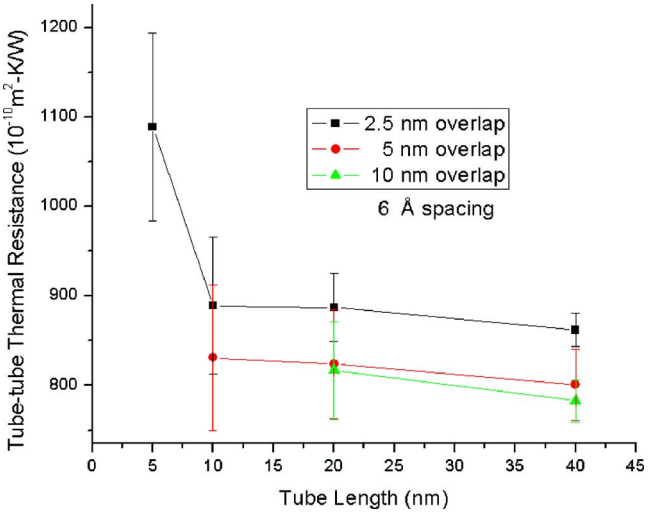

FIG. 7. (Color online) Tube-tube thermal resistance vs tube length for 5, 10, 20, and 40 nm tubes with 2.5 nm overlap and 6 Å spacing. Resistance decreases as tube length increases.

interactions. For many of the above results in Figs. 5 and 7, overlapping error bars prevent full separation of resistance values for some of the cases of spacing, overlap, or length. The totality of the data suggests, however, that there are clear reductions in tube-tube resistance with longer length, bigger overlap, and smaller spacing.

VI. EFFECT OF PARAMETERIZATION ON TUBE-TUBE RESISTANCE

The nonbonded interaction between nanotubes dominates the tube-tube interfacial thermal resistances calculated in Sec. V. As discussed in Sec. II, several different functional forms and parameterizations have been utilized in the literature to model this interaction. These differences, then, are expected to influence the interfacial resistances to some degree. Here an analysis is performed for the LJ interaction to determine the effects of ε and σ on the obtained tube-tube interfacial thermal resistances. This analysis is based on the law of corresponding states for the thermal conductivity of molecular LJ solids,[51] and on conversion of Kapitza conductance of the interface, G, into interfacial resistance. The law of corresponding states rests on the fact that physical properties of all LJ materials can be reduced to a universal curve through nondimensionalization. Hence, calculations need only be run for one parameterization, and the results can be converted to that of any other parameterization using a simple scaling factor. The nondimensionalized thermal conductivity k^* is found by dividing thermal conductivity by a characteristic thermal conductivity k_{char},

$$k^* = \frac{k}{k_{char}}, \tag{8}$$

where k_{char} is defined as[51,52]

$$k_{char} = \frac{k_B}{\sigma^2}\sqrt{\frac{\varepsilon}{m}}, \tag{9}$$

and m and k_B are the atomic mass and Boltzmann's constant, respectively.

The interfacial thermal resistance is related to conductivity as follows

$$R = \frac{1}{G} = \frac{d}{k} = \frac{d}{k_{char}k^*} = \frac{d\sigma^2}{k^* k_B}\sqrt{\frac{m}{\varepsilon}}. \tag{10}$$

In Eq. (10), conductance is defined in the traditional way as effective thermal conductivity (k) divided by the length through which heat flows (d). As applied to the present situation, d corresponds to the tube-tube spacing and k to an effective thermal conductivity. If R_o is the resistance for a reference parameterization (ε_o, σ_o), the resistance for any arbitrary parameterization (ε, σ) is given by

$$R = \left[\frac{\sigma^2}{\sigma_o^2}\sqrt{\frac{\varepsilon_o}{\varepsilon}}\right]R_o. \tag{11}$$

This simple equation can be used to scale the tube-tube resistances reported in Figs. 2, 5, 6(a), and 7 to those of any of the various LJ parameterizations discussed above. For example, taking the reference parameterization (ε_o=2.4 meV, σ_o=0.34 nm) and the parameterization used by Lu *et al.*[33] and in the present work (ε=4.41 meV, σ=0.228 nm), we invert Eq. (11) to obtain $R_o/R \approx 3$. This is consistent with our order of magnitude agreement with the values of Huxtable *et al.*[12] and Maruyama *et al.*[11]

VII. RESERVOIR-TUBE INTERFACIAL RESISTANCES

Reservoir-tube resistances are also calculated using the above method (Fig. 8). As with the tube-tube resistances, convergence studies reveal no dependence on the particular fitting snapshot used (Fig. 6(b)). There is also no dependence on the Nosé-Hoover thermostat parameter (Fig. 9). The resistances are found to be about 13–60 times larger than the intrinsic resistances of single nanotubes, but about 600–700 times smaller than tube-tube thermal resistances. Intrinsic thermal resistances are defined as $\Delta x/k$, where Δx=2.46 Å is the distance between two adjacent rings of atoms in one carbon nanotube, and k is the thermal conductivity corresponding to the particular nanotube length.[46,48] The reservoir-tube resistance at the cold end R_C is larger than that at the hot end R_H, with some slight overlapping of error bars due to the fairly small (40 K) temperature difference applied. As above, it is believed that the data taken together indicate a clear temperature dependence of reservoir-tube resistance. The increase is consistent with predictions of increased boundary resistance at low temperatures from diffuse mismatch theory,[43] but rigorous assessment of temperature dependence is not possible presently since there are only two data points for temperatures treated here. The reservoir-tube resistance decreases with nanotube length.

To see how phonons are coupled across the reservoir-tube interface, the full phonon density of states (DOS) $D(\omega)$ is

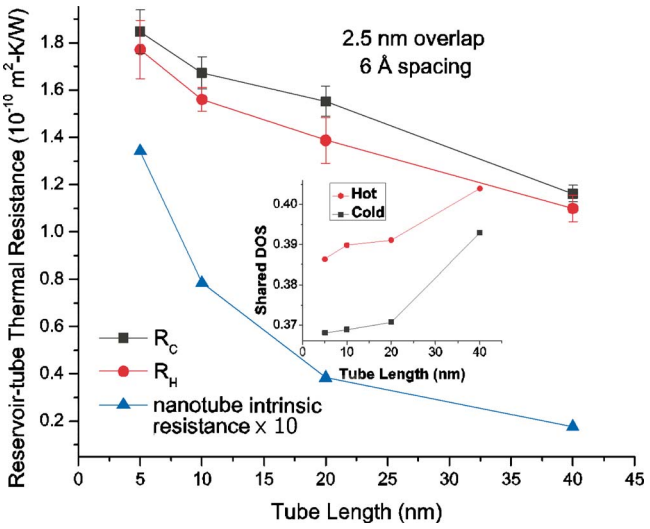

FIG. 8. (Color online) Hot reservoir-tube, cold reservoir-tube, and nanotube intrinsic thermal resistances vs tube length for 5, 10, 20, and 40 nm tubes with 2.5 nm overlap and 6 Å spacing. Nanotube intrinsic resistance is multiplied by ten for plotting purposes. Shared density of states is in arbitrary units. Resistances decrease as tube length increases. The cold reservoir-tube resistance is higher than the hot reservoir-tube resistance; the shared density of states is higher at the hot end. Reservoir-tube resistances are higher than intrinsic resistance.

calculated for a reservoir and for its adjacent nonthermostatted region as

$$D(\omega) = F\int dt e^{-i\omega t}\langle \vec{v}(t)\cdot\vec{v}(0)\rangle \tag{12}$$

where F is a normalization factor set equal to one and the quantity in brackets represents the velocity autocorrelation function. This function is calculated separately for the reservoirs and neighboring regions from the particle velocities in the respective regions. All four regions are of the same

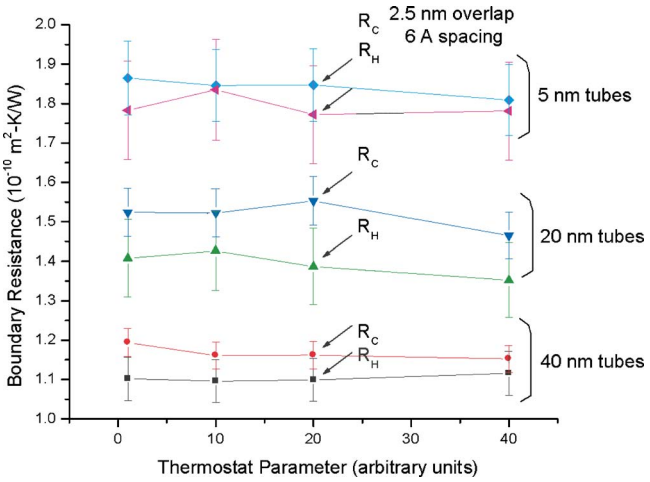

FIG. 9. (Color online) Tube-reservoir resistance dependence on Nosé-Hoover thermostat parameter. Within error, the resistances are independent of thermostat parameter.

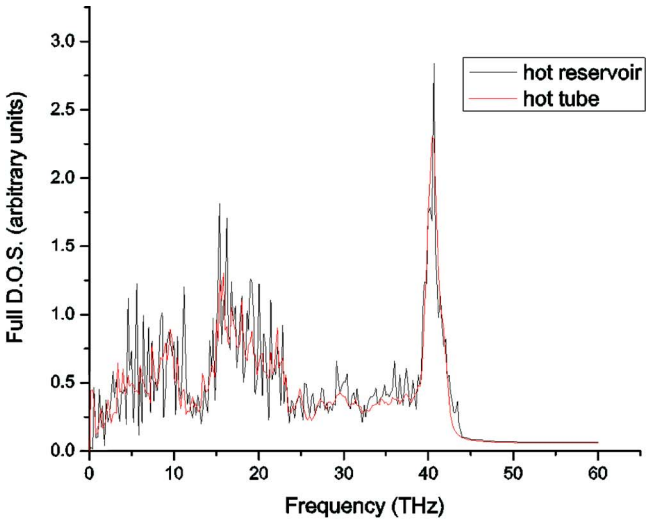

(a)

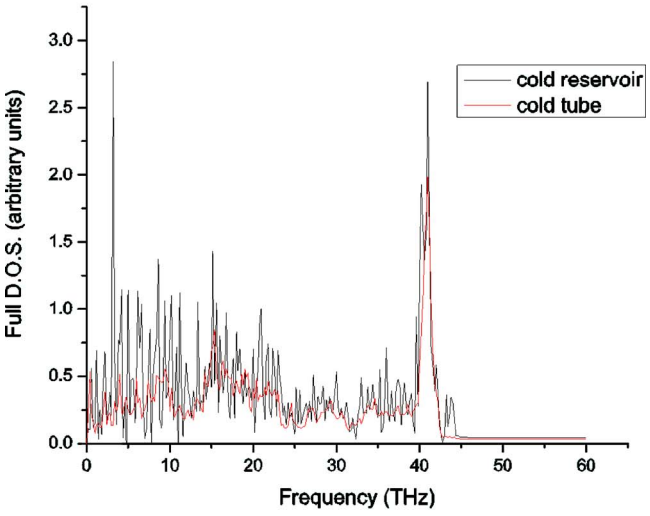

(b)

FIG. 10. (Color online) Full density of states calculated for a reservoir and for its adjacent nonthermostatted region for (a) hot and (b) cold ends of the two-nanotube system. The common area under reservoir and tube curves is defined here as the shared density of states.

length, 1.25 nm. The Fourier transform is then taken for each region using 4000 temporal points to obtain the DOS. Example DOS curves are plotted in Fig. 10(a) for the hot reservoir and the nanotube region nearest the hot reservoir and in Fig. 10(b) for the cold reservoir and the nanotube region nearest the cold reservoir. The common area under the reservoir and tube curves, or the shared DOS, is calculated as a rough measure of the tube-tube coupling: higher shared DOS indicates lower thermal resistance. This is done for both hot and cold ends of the nanotube, and the results are shown in the inset of Fig. 8. For both cases, the shared DOS increases with nanotube length. As in the tube-tube case, it is believed that longer nanotubes have more coupled modes that can

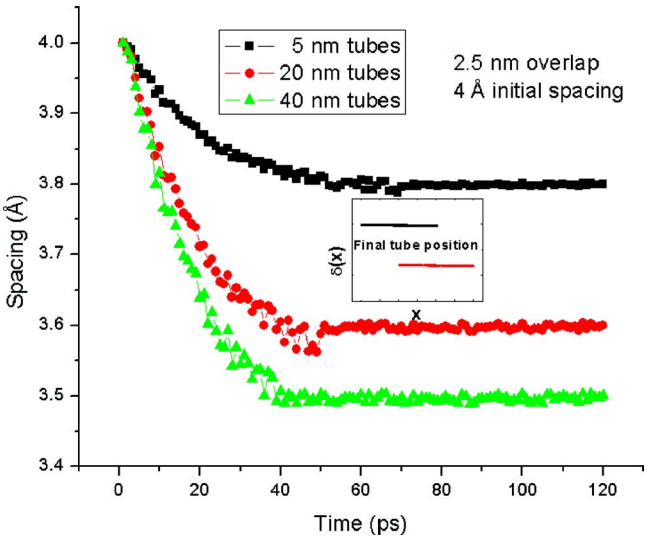

FIG. 11. (Color online) Spacing between free nanotube ends vs time for 5, 20, and 40 nm nanotubes with 2.5 nm overlap and 4 Å initial spacing. Shorter nanotubes are more highly damped than longer nanotubes and reach steady state later.

cross the reservoir-tube interface and therefore result in lower reservoir-tube resistances. The hot reservoir-tube shared DOS is always larger than the cold reservoir-tube shared DOS, which is consistent with the increased reservoir-tube thermal resistance at lower temperatures shown in Fig. 8. From the simulation data there is no evidence that spacing and overlap affect reservoir-tube resistances.

VIII. NANOTUBE BENDING

For 4 Å or larger initial spacings, the free ends of the two nanotubes are observed to approach each other over time due to interactions in the overlap region. Figure 11 shows the dynamics of end-end spacing and the inset shows the final atomic positions of both nanotubes. How much displacement the nanotube ends make depends on initial spacing, overlap, and length, but in all cases the deflection is less than 0.2% of the total nanotube length so that the nanotubes can still be considered straight. More overlap or smaller initial spacing gives stronger interaction and therefore makes the final spacing between the nanotube ends smaller. Longer nanotubes bend more, attain steady state more quickly, and also display a smaller final spacing between the free ends. The final steady-state spacing for all cases investigated is achieved at around 70 ps. The above-described MD/finite difference fitting to determine thermal resistances is only performed after this time.

To eliminate bending as a possible cause of the length-dependent thermal resistance, additional calculations on tubes with both ends fixed were performed. The resistances for the fixed-fixed case were slightly higher than for the fixed-free case but were the same within error. Decreases in resistance with decreased spacing, increased overlap, and increased length were still observed for the fixed-fixed case,

TABLE I. Young's modulus of individual (10, 10) single-wall carbon nanotubes.

	Tube length (nm)	Method	E (TPa)
Present work	5–40	Eqs. (13)–(15)	1.15–1.42
	High value (TPa)	Low value (TPa)	Mid-range value (TPa)
Experimental	2.8–3.6[a]	0.32–1.47[b]	1.26–1.36[c]
Theoretical/ computational	4.5[d]	0.405–0.705[e]	1.24[f] 1.35[g]

[a]Reference 30.
[b]Reference 31.
[c]Reference 32.
[d]Reference 33.
[e]Reference 34.
[f]Reference 35.
[g]Reference 36.

indicating that the slight bending had no significant effect on the results.

IX. YOUNG'S MODULI AND DAMPING COEFFICIENTS

The steady-state bending of the nanotube ends can be used to obtain a simple estimate of Young's modulus, E. Assuming uniform loading p over a finite length a at the end of a hollow tube cantilever, Young's modulus can be calculated from[53]

$$\delta = \frac{p}{24EI}(a^4 - 6a^2l^2 + 8al^3), \tag{13}$$

$$I = \frac{\pi d^3 t}{8}, \tag{14}$$

where δ is the displacement of the tip of the nanotube, I is the moment of inertia, l is the length, d is the diameter, and t is the nanotube thickness. Here $d=1.356$ nm, t is taken as the interlayer spacing of graphite (0.34 nm), and p is calculated by molecular dynamics from the average of initial and final interaction forces in the overlap area. Calculated values of E are shown in Table I along with other literature values for carbon nanotubes.[21–23,54–59] Our calculated values agree very well with those of earlier experimental and theoretical studies. More importantly, they decrease with nanotube length. This length dependence has not been reported previously for carbon nanotubes. A related result has been found in recent molecular dynamics simulations of gold nanowires: E was found to decrease with aspect ratio, although length effects were not specifically considered.[60]

In order to understand why longer nanotubes reach steady state more quickly (Fig. 11), the differential equation for cantilever deflection[61] is studied,

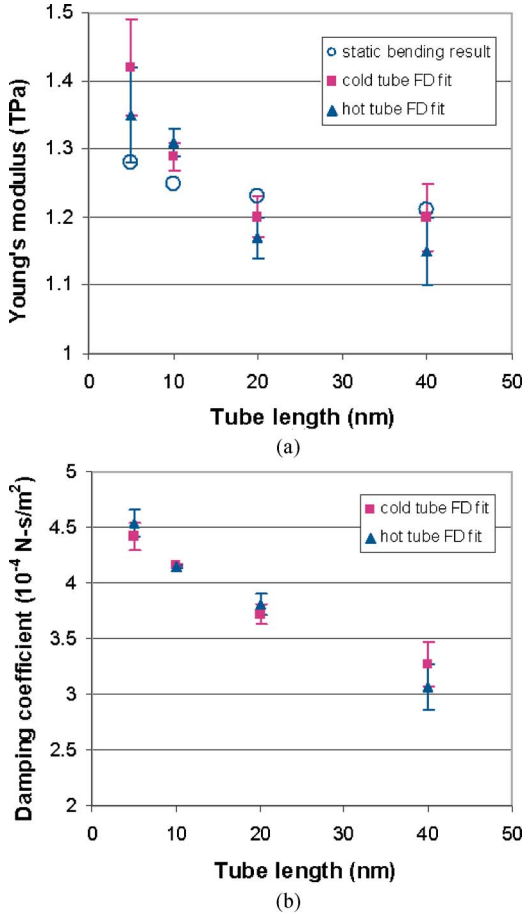

FIG. 12. (Color online) (a) Young's modulus and (b) damping coefficient vs tube length. Both Young's modulus and damping coefficient decrease with increasing length.

$$EI\frac{\partial^4 y}{\partial x^4} + m\frac{\partial^2 y}{\partial t^2} + C\frac{\partial y}{\partial t} = f(x,t) \tag{15}$$

where $y=y(x,t)$ is the deflection, E is Young's modulus, I is the moment of inertia, m is the mass per unit length, C is the damping coefficient, and $f(x,t)$ is the external force per unit length. The solution to Eq. (15) is fit to transient bending curves from molecular dynamics simulation to obtain both Young's modulus and damping coefficient using snapshots in a similar procedure to that described in Sec. IV. The external forces used in Eq. (15) are obtained from molecular dynamics. This fitting method provides a more accurate means of obtaining E and C than the static deflection method of Eq. (13) because it utilizes the deflection curve of the entire nanotube rather than the deflection at a single point (the nanotube tip), and because the actual, nonuniform loading rather than an assumed uniform loading is employed in the right-hand side of Eq. (15).

The results for E and C are shown in Fig. 12. Error in E and C is estimated as the difference between values obtained from finite difference fitting of the deflection equations of hot and cold nanotubes. In Fig. 12(a), it is seen that the Young's moduli calculated using this transient fitting method on both hot and cold nanotubes decrease with length and

agree well with those obtained from the static method; the values also agree well with those from the literature (Table I). The damping coefficient C decreases with length, which is consistent with experimentally measured damping coefficients of lead zirconate titanate (PZT) cantilevers[62] and quality factors in silicon resonators.[63]

X. CONCLUSION

Thermal interfacial resistances between carbon nanotubes and between carbon nanotubes and constant temperature nanotube reservoir regions have been investigated for various (10,10) nanotube configurations. Increasing tube-tube contact dramatically reduces interfacial resistance. Molecular dynamics simulations reveal transient motion of the free ends of the nanotubes. From the steady-state and transient deflection curves, Young's moduli and damping coefficients that decrease with nanotube length are found.

ACKNOWLEDGMENT

This work was supported by the Office of Naval Research, Grant No. N00014-03-1-0890.

*Electronic address: jrlukes@seas.upenn.edu

[1] C. H. Yu, L. Shi, Z. Yao, D. Y. Li, and A. Majumdar, Nano Lett. **5**, 1842 (2005).
[2] S. Berber, Y. K. Kwon, and D. Tomanek, Phys. Rev. Lett. **84**, 4613 (2000).
[3] M. A. Osman and D. Srivastava, Nanotechnology **12**, 21 (2001).
[4] J. Che, T. Çagin, and W. A. Goddard III, Nanotechnology **11**, 65 (2000).
[5] C. W. Padgett and D. W. Brenner, Nano Lett. **4**, 1051 (2004).
[6] J. F. Moreland, J. B. Freund, and G. Chen, Microscale Thermophys. Eng. **8**, 61 (2004).
[7] S. Maruyama, Microscale Thermophys. Eng. **7**, 41 (2003).
[8] F. M. Du, J. E. Fischer, and K. I. Winey, J. Polym. Sci., Part B: Polym. Phys. **41**, 3333 (2003).
[9] H. F. Chuang, S. M. Cooper, M. Meyyappan, and B. A. Cruden, J. Nanosci. Nanotechnol. **4**, 964 (2004).
[10] S. Shenogin, L. Xue, R. Ozisik, P. Keblinski, and D. G. Cahill, J. Appl. Phys. **95**, 8136 (2004).
[11] S. Maruyama, Y. Igarashi, Y. Taniguchi, and Y. Shibuta, in *Proceedings of the 1st International Symposium on Micro and Nano Technology*, edited by M. Inoue (Pacific Center of Thermal-Fluids Engineering, 2004).
[12] S. T. Huxtable, D. G. Cahill, S. Shenogin, L. Xue, R. Ozisik, P. Barone, M. Usrey, M. S. Strano, G. Siddons, M. Shim, and P. Keblinski, Nat. Mater. **2**, 731 (2003).
[13] F. Du, R. C. Scogna, W. Zhou, S. Brand, J. E. Fischer, and K. I. Winey, Macromolecules **37**, 9048 (2004).
[14] J. Loos, A. Alexeev, N. Grossiord, C. E. Koning, and O. Regev, Ultramicroscopy **104**, 160 (2005).
[15] A. G. Rinzler, J. Liu, H. Dai, P. Nikolaev, C. B. Huffman, F. J. Rodríguez-Macias, P. J. Boul, A. H. Lu, D. Heymann, D. T. Colbert, R. S. Lee, J. E. Fischer, A. M. Rao, P. C. Eklund, and R. E. Smalley, Appl. Phys. A: Mater. Sci. Process. **67**, 29 (1998).
[16] S. Sapmaz, P. Jarillo-Herrero, Y. M. Blanter, C. Dekker, and H. S. J. van der Zant, Phys. Rev. Lett. **96**, 026801 (2006).
[17] J. Hone, M. Whitney, C. Piskoti, and A. Zettl, Phys. Rev. B **59**, R2514 (1999).
[18] H. B. Peng, T. G. Ristroph, G. M. Schurmann, G. M. King, J. Yoon, V. Narayanamurti, and J. A. Golovchenko, Appl. Phys. Lett. **83**, 4238 (2003).
[19] Y. Li, W. Kim, Y. Zhang, M. Rolandi, D. Wang, and H. Dai, J. Phys. Chem. B **105**, 11424 (2001).
[20] V. Sazonova, Y. Yaish, H. Ustunel, D. Roundy, T. A. Arias, and P. L. McEuen, Nature (London) **431**, 284 (2004).
[21] R. S. Ruoff, D. Qian, and W. K. Liu, C. R. Phys. **4**, 993 (2003).
[22] H. W. Zhang, J. B. Wang, and X. Guo, J. Mech. Phys. Solids **53**, 1929 (2005).
[23] E. Hernández, C. Goze, P. Bernier, and A. Rubio, Phys. Rev. Lett. **80**, 4502 (1998).
[24] E. Hernández, C. Goze, P. Bernier, and A. Rubio, Appl. Phys. A: Mater. Sci. Process. **68**, 287 (1999).
[25] C. Li and T.-W. Chou, Compos. Sci. Technol. **63**, 1517 (2003).
[26] M. P. Allen and D. J. Tildesley, *Computer Simulation of Liquids* (Clarendon Press, Oxford, 1987).
[27] M. S. Dresselhaus and P. C. Eklund, Adv. Phys. **49**, 705 (2000).
[28] D. W. Brenner, O. A. Shenderova, J. A. Harrison, S. J. Stuart, B. Ni, and S. B. Sinnott, J. Phys. Condens. Matter **14**, 783 (2002).
[29] L. A. Girifalco, M. Hodak, and R. S. Lee, Phys. Rev. B **62**, 13104 (2000).
[30] Y. Wang, D. Tomanek, and G. F. Bertsch, Phys. Rev. B **44**, 6562 (1991).
[31] D. Qian, W. K. Liu, and R. S. Ruoff, J. Phys. Chem. B **105**, 10753 (2001).
[32] G. Garberoglio, M. M. DeKlavon, and J. K. Johnson, J. Phys. Chem. B **110**, 1733 (2006).
[33] T. Lu, E. M. Goldfield, and S. K. Gray, J. Phys. Chem. B **107**, 12989 (2003).
[34] S. B. Sinnott, O. A. Shenderova, C. T. White, and D. W. Brenner, Carbon **36**, 1 (1998).
[35] A. K. Rappe, C. J. Casewit, K. S. Colwell, W. A. Goddard III, and W. M. Skiff, J. Am. Chem. Soc. **114**, 10024 (1992).
[36] J. H. Walther, R. Jaffe, T. Halicioglu, and P. Koumoutsakos, J. Phys. Chem. B **105**, 9980 (2001).
[37] P. K. Schelling and P. Keblinski, Phys. Rev. B **68**, 035425 (2003).
[38] J. P. Lu, Phys. Rev. Lett. **79**, 1297 (1997).
[39] W. G. Hoover, Phys. Rev. A **31**, 1695 (1985).
[40] P. L. Kapitza, J. Phys. (USSR) **4**, 181 (1941).
[41] W. A. Little, Can. J. Phys. **37**, 334 (1959).
[42] G. L. Pollack, Rev. Mod. Phys. **41**, 48 (1969).
[43] E. T. Swartz and R. O. Pohl, Rev. Mod. Phys. **61**, 605 (1989).
[44] Z. Yao, J. Wang, B. Li, and G. Liu, Phys. Rev. B **71**, 085417 (2005).
[45] J. Hone, B. Batlogg, Z. Benes, A. T. Johnson, and J. E. Fischer, Science **289**, 1730 (2000).
[46] H. Zhong and J. R. Lukes, in *Proceedings of the 2004 International Mechanical Engineering Congress and Exposition*,

IMECE2004-61665 (ASME, 2004).
[47] N. Mingo and D. A. Broido, Nano Lett. **5**, 1221 (2005).
[48] H. Zhong and J. R. Lukes (unpublished).
[49] P. S. Ghoshdastidar, *Heat Transfer* (Oxford University Press, Oxford, 2004).
[50] S. Mazumder and A. Majumdar, J. Heat Transfer **123**, 749 (2001).
[51] R. W. Keyes, J. Chem. Phys. **31**, 452 (1959).
[52] J. R. Lukes, D. Y. Li, X.-G. Liang, and C.-L. Tien, J. Heat Transfer **122**, 536 (2000).
[53] R. R. Craig, *Structural Dynamics* (John Wiley and Sons, New York, 1981).
[54] O. Lourie and H. D. Wagner, J. Mater. Res. **13**, 2418 (1998).
[55] M.-F. Yu, O. Lourie, M. J. Dyer, K. Moloni, T. F. Kelly, and R. S. Ruoff, Science **287**, 637 (2000).
[56] A. Krishnan, E. Dujardin, T. W. Ebbesen, P. N. Yianilos, and M. M. J. Treacy, Phys. Rev. B **58**, 14013 (1998).
[57] B. I. Yakobson, C. J. Brabec, and J. Bernholc, Phys. Rev. Lett. **76**, 2511 (1996).
[58] H. Jiang, P. Zhang, B. Liu, Y. M. Huang, P. H. Geubelle, H. Gao, and K. C. Hwang, Comput. Mater. Sci. **28**, 429 (2003).
[59] Y. Jin and F. G. Yuan, Compos. Sci. Technol. **63**, 1507 (2003).
[60] J.-S. Lin, S.-P. Ju, and W.-J. Lee, Phys. Rev. B **72**, 085448 (2005).
[61] W. Zhang and K. L. Turner, Sensors, 2005 IEEE, pp. 357–360 (2005).
[62] C. Lee, T. Itoh, R. Maeda, and T. Suga, Rev. Sci. Instrum. **68**, 2091 (1997).
[63] P. Mohanty, D. A. Harrington, K. L. Ekinci, Y. T. Yang, M. J. Murphy, and M. L. Roukes, Phys. Rev. B **66**, 085416 (2002).